ORIGINAL ARTICLE   OPEN

The immune checkpoint TIGIT is upregulated on T cells during bacterial infection and is a potential target for immunotherapy

Timothy R McCulloch[1,a] 🆔 🐦, Gustavo R Rossi[1,a] 🐦, Socorro Miranda-Hernandez[2], Ana Maria Valencia-Hernandez[3], Louisa Alim[1], Clemence J Belle[1], Andrew Krause[4], Lucia F Zacchi[4], Pui Yeng Lam[1], Kyohei Nakamura[5] 🆔, Andreas Kupz[3,b], Timothy J Wells[1,6,b] & Fernando Souza-Fonseca-Guimaraes[1,b] 🆔 🐦

1 Frazer Institute, Faculty of Medicine, The University of Queensland, Woolloongabba, QLD, Australia
2 Australian Institute of Tropical Health and Medicine, James Cook University, Townsville, QLD, Australia
3 Australian Institute of Tropical Health and Medicine, James Cook University, Cairns, QLD, Australia
4 Australian Institute for Bioengineering and Nanotechnology, The University of Queensland, St Lucia, QLD, Australia
5 QIMR Berghofer Medical Research Institute, Herston, QLD, Australia
6 Australian Infectious Diseases Research Centre, University of Queensland, Brisbane, QLD, Australia

Abstract

Antibiotic resistance is a major public health threat, and alternatives to antibiotic therapy are urgently needed. Immunotherapy, particularly the blockade of inhibitory immune checkpoints, is a leading treatment option in cancer and autoimmunity. In this study, we used a murine model of *Salmonella* Typhimurium infection to investigate whether immune checkpoint blockade could be applied to bacterial infection. We found that the immune checkpoint T-cell immunoglobulin and ITIM domain (TIGIT) was significantly upregulated on lymphocytes during infection, particularly on CD4^{+} T cells, drastically limiting their proinflammatory function. Blockade of TIGIT *in vivo* using monoclonal antibodies was able to enhance immunity and improve bacterial clearance. The efficacy of anti-TIGIT was dependent on the capacity of the antibody to bind to Fc (fragment crystallizable) receptors, giving important insights into the mechanism of anti-TIGIT therapy. This research suggests that targeting immune checkpoints, such as TIGIT, has the potential to enhance immune responses toward bacteria and restore antibacterial treatment options in the face of antibiotic resistance.

INTRODUCTION

Bacterial infections represent a major burden of disease worldwide, which is set to worsen in the face of the developing antimicrobial resistance crisis. In 2019, antibiotic-resistant bacteria were estimated to be associated with 4.87 million global deaths, of which 1.27 million were directly attributable to antibiotic resistance.[1] New therapies to address bacterial infection and subsequent complications such as sepsis are a global health priority, and immunotherapy is emerging as a potential alternative or adjunct to traditional antimicrobial therapy.[2,3]

Immunotherapy takes advantage of the host's immune system to combat disease. A prominent example is an immune checkpoint inhibitor. During pathological conditions such as infection and cancer, immune cells upregulate inhibitory receptors called immune checkpoints. When immune checkpoints interact with their ligand, they mitigate inflammatory immune responses and restrict immune-mediated pathology. However, this can also prevent control of infection or malignancy. Blockade of immune checkpoints through monoclonal antibodies prevents the receptor–ligand interaction, thus restoring immune responses.[3–5] The foremost examples of immune checkpoint inhibitors at

present are anti–programmed cell death protein-1 (PD-1)[6] and anti–cytotoxic T-lymphocyte–associated protein-4 (CTLA-4),[7] which are both routinely used in cancer therapy. However, new targets such as lymphocyte-activating gene-3 (Lag-3), T-cell immunoglobulin and mucin domain 3 (Tim-3) and T-cell immunoreceptor with T-cell immunoglobulin and ITIM domain (TIGIT) are showing promise as the next-generation immune checkpoint inhibitor.[8]

TIGIT is a co-inhibitory receptor of the immunoglobulin superfamily, expressed on activated T and natural killer cells. TIGIT functions through the binding of its ligands, CD155 and CD112, which are present on antigen-presenting cells and tumor cells.[9] The expression of TIGIT and its binding to CD155/CD112 has immunoregulatory consequences, which are thought to occur through several mechanisms: polarization of dendritic cells toward a tolerogenic phenotype, reducing interleukin-12 (IL-12) and promoting IL-10 production[10]; disruption of CD226 homodimerization and thus functional expression[11]; outcompeting CD226 binding[11]; direct inhibitory signals to the TIGIT expressing lymphocyte[12] and enhancing suppressive functions of regulatory T cells.[13] The nuances of these mechanisms and whether they are cell-type or pathology dependent are yet to be determined. Regardless, the findings of immunoregulation have uncovered TIGIT as a promising target for immune checkpoint inhibitor in cancer, particularly when used in combination with other inhibitors such as anti–PD-1.[14]

Previous evidence suggested that TIGIT might play a role in viral infections such as influenza,[15] lymphocytic choriomeningitis virus[11] and HIV,[16] as well as fungal infections such as invasive *Candida albicans* infection.[17] However, the role of TIGIT in bacterial infections and whether it is a viable target remain unknown. In this study, we found that TIGIT acts as an inhibitory immune checkpoint during *Salmonella enterica* serovar Typhimurium (*S.* Typhimurium) infection. Further, anti-TIGIT therapy promoted bacterial clearance, suggesting TIGIT may be a potential immunotherapy target in bacterial infections.

RESULTS

TIGIT is an inhibitory receptor on CD4⁺ T cells during *S.* Typhimurium infection

To investigate how immune checkpoints may regulate immunity during invasive bacterial infection, wild-type (WT) C57BL/6 mice were infected with *S.* Typhimurium

by intraperitoneal injection and immune checkpoint upregulation on effector lymphocyte populations was examined 10 days postinfection (Figure 1a). We identified substantial differences between naïve and infected mice (Figure 1b), characterized by upregulation of checkpoints Tim-3, Lag-3 and TIGIT on both $CD4^+$ and $CD8^+$ T cells in the spleen of infected mice (Supplementary figure 1a). The most upregulated immune checkpoint was TIGIT, which was upregulated on the majority of $CD4^+$ T cells (Figure 1b). TIGIT was upregulated on both $FoxP3^-$ conventional $CD4^+$ T cells (T_{conv}) and $FoxP3^+$ regulatory $CD4^+$ T cells (T_{reg}; Figure 1c). To assess the temporal dynamics of TIGIT expression, we examined mice at different time points postinfection. Of note, $TIGIT^+$ T_{conv} were the most numerous TIGIT-expressing cell type examined, peaking in numbers at day 7 postinfection before reducing as the infection resolved by day 28 (Figure 1d). Considering the importance of $CD4^+$ T-cell responses in antibacterial immunity,[18] we predicted that $CD4^+$ T_{conv} cells would be the primary cell type impacted by TIGIT upregulation. When comparing $TIGIT^-$ with $TIGIT^+$ $CD4^+$ T_{conv} cells from infected mice, we found that $TIGIT^+$ cells expressed CD44 and lacked CD62L, indicating they were effector/memory T cells (Supplementary figure 1c). $TIGIT^+$ cells also expressed higher levels of co-inhibitory molecules including Tim-3 and Lag-3, as well as the activation marker CD69, and proliferation marker Ki-67 (Supplementary figure 1c). When examining the T-cell receptor repertoire by flow cytometry, there appeared to be no difference in T-cell receptor proportions between $CD4^+$ T cells from naïve or infected mice (Supplementary figure 1d), and only minimal differences between $TIGIT^-$ and $TIGIT^+$ cells from infected mice (Supplementary figure 1e), suggesting that upregulation of TIGIT was unlikely a result of expansion of antigen-specific clones.

To assess functional changes in response to TIGIT upregulation, $CD4^+$ T cells were taken from naïve or infected mice and stimulated with plate-bound anti-CD3 and anti-CD28 in the presence of CD155-Fc (the ligand of TIGIT) or an isotype control. After 24 h, cytokine production was analyzed by flow cytometry (Figure 1e). While no differences were observed in tumor necrosis factor production (Supplementary figure 1f), $CD4^+$ T cells exposed to CD155 expressed significantly less interferon gamma (IFNγ) compared with controls (Figure 1f). Reductions in IFNγ levels were corroborated by ELISA, where we observed significantly less IFNγ in supernatants of CD155-treated T cells compared with isotype control (Figure 1g). Conversely, IL-10 is a
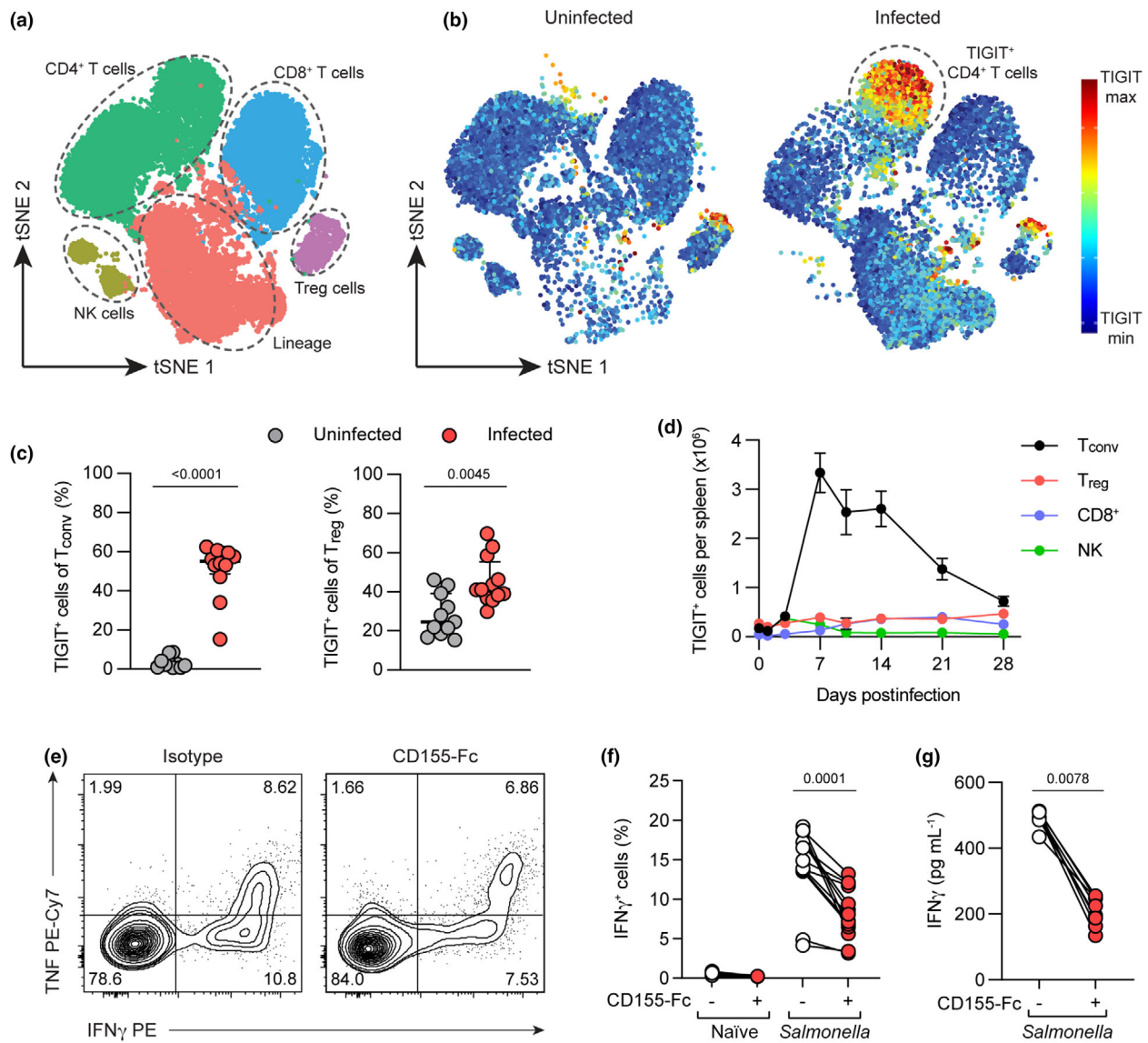
Figure 1. TIGIT is an inhibitory receptor on CD4$^+$ T cells during *S.* Typhimurium infection. Upregulation of immune checkpoints on splenic lymphocytes was analyzed by multiparametric flow cytometry 10 days after infection with *S.* Typhimurium. **(a)** tSNE analysis showing lymphocyte clusters and **(b)** differences in TIGIT expression from uninfected and infected mice. Each dot represents an individual cell. **(c)** TIGIT expression on T$_{conv}$ (CD45$^+$CD3$^+$CD4$^+$FoxP3$^-$) and T$_{reg}$ (CD45$^+$CD3$^+$CD4$^+$FoxP3$^+$) from uninfected and infected mice. **(d)** TIGIT expression was measured at various time points postinfection; total numbers of TIGIT$^+$ NK, T$_{conv}$, CD8$^+$ and T$_{reg}$ shown over 28 days. CD4$^+$ T cells isolated from either naïve or *S.* Typhimurium–infected mice were stimulated for 24 h with plate-bound anti-CD3 and anti-CD28 in the presence of plate-bound CD155-Fc or isotype control. **(e)** Representative flow cytometry plots showing expression of TNF and IFNγ in CD4$^+$ T cells from infected mice. **(f)** Percentage of cells expressing IFNγ. **(g)** IFNγ titers from culture supernatant. Data are from two independent experiments (**a–c**, $n = 14$; **d**, $n = 8$–0; **e–g**, $n = 11$–14). Each symbol represents an individual mouse. Graphs show median ± interquartile range for **c**, or mean value ± standard error of the mean for **(d)**. Groups were compared by the Mann–Whitney *U*-test with Benjamini, Krieger and Yekutieli adjustment for multiple comparisons for **(c)**, or the Wilcoxon matched-pairs test for **(f)** and **(g)**, where $P < 0.05$ was considered significantly different. Fc, fragment crystallizable; IFNγ, interferon gamma; NK, natural killer; T$_{conv}$, conventional T cells; T$_{reg}$, regulatory T cells; TIGIT, T-cell immunoglobulin and ITIM domain; TNF, tumor necrosis factor; tSNE, t-distributed stochastic neighbor embedding.

key suppressive factor promoting *S.* Typhimurium infection,[19] and TIGIT ligation is also thought to trigger IL-10 production.[10,20] However, we could not detect IL-10 production in any condition. Together, these data show that TIGIT is an inhibitory receptor of CD4$^+$ T cells during *S.* Typhimurium infection.
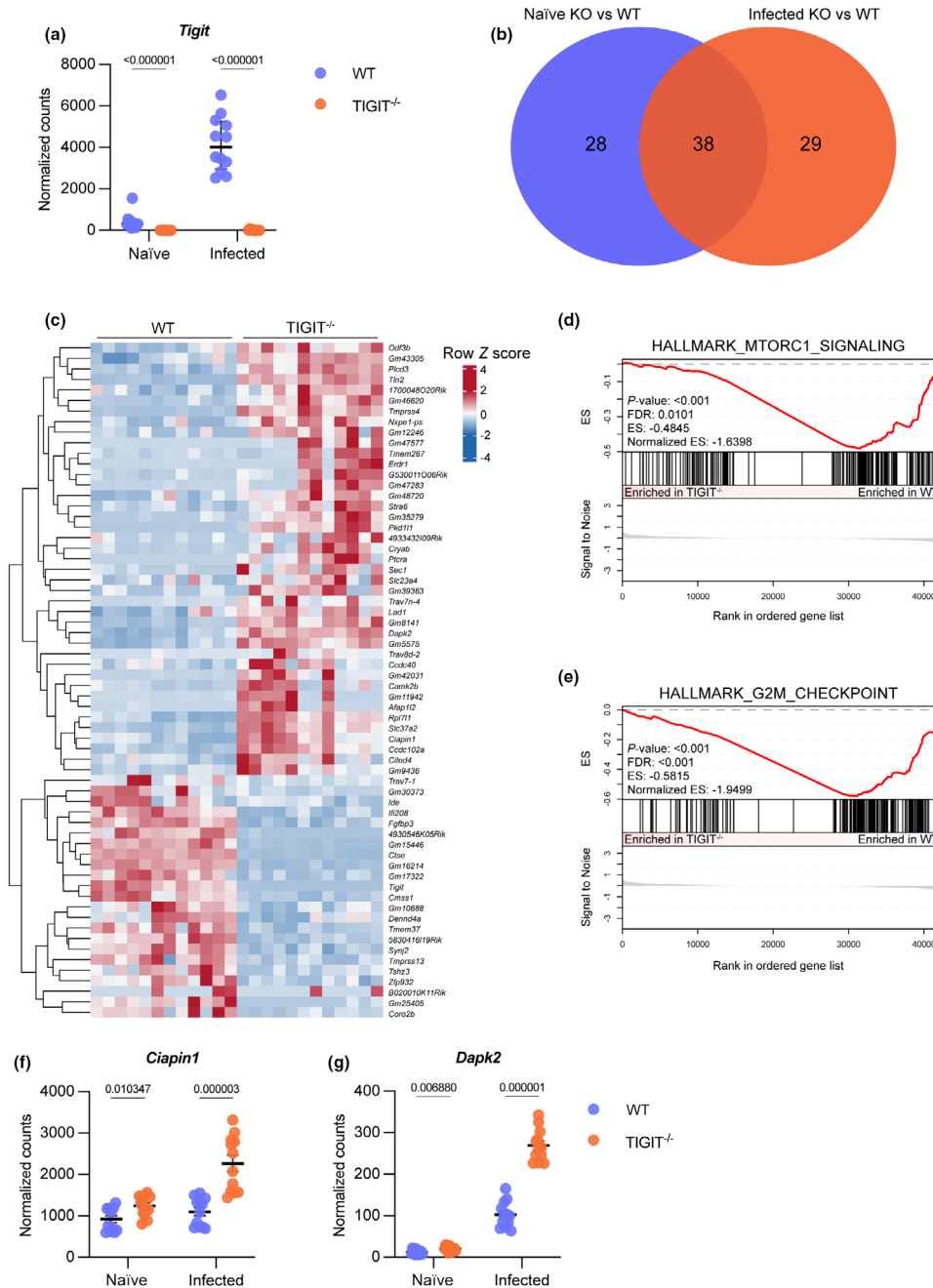
TIGIT induces transcriptional changes in CD4⁺ T cells

We predicted that TIGIT may be inducing functional changes in CD4⁺ T cells by regulating gene transcription. To assess this, we generated bone marrow chimeric mice using a 50:50 mix of bone marrow from WT and *TIigit⁻/⁻* mice (Supplementary figure 2a), allowing us to assess the direct effects of TIGIT on T cells without secondary effects of dendritic cells or other CD155-expressing cells. Chimera mice were infected with *S.* Typhimurium, then WT or *Tigit⁻/⁻* CD4⁺ T cells were isolated and processed for bulk RNA-sequencing. Expression of *Tigit* was absent in the *Tigit⁻/⁻* cells (Figure 2a), validating our knockout model. When comparing WT with *Tigit⁻/⁻* cells, there were 66 differentially expressed genes between naïve WT and *Tigit⁻/⁻* cells ($P_{adj} < 0.05$ and $\log_2 FC > 0.58$), and 67 differentially expressed genes between infected WT and *Tigit⁻/⁻* ($P_{adj} < 0.05$ and $\log_2 FC > 0.58$). Of these genes, 38 were shared between T cells from naïve and infected mice, while 29 were unique to infected T cells (Figure 2b), suggesting that upregulation of TIGIT can lead to transcriptional changes specifically in the context of bacterial infection. Upregulated genes in *Tigit⁻/⁻* CD4⁺ T cells compared with WT cells from infected mice included genes associated with nutrient uptake (*Slc37a2*, *Slc23a4* and *Stra6*), as well as apoptosis/cell death (*Erdr1*, *Ciapin1* and *Dapk2*; Figure 2c). Curiously, Gene Set Enrichment Analysis showed enrichment of both mammalian target of rapamycin complex 1 (mTORC1) signaling (Figure 2d) and G2M checkpoint (Figure 2d) in infected WT cells compared with *Tigit⁻/⁻*, going against the hypothesis that TIGIT is strictly an inhibitory marker on T cells. It is possible that expression of TIGIT helps to restrain the overactivation of T cells in certain contexts, and its deletion contributes to activation-induced cell death. This would be consistent with our findings of upregulation of cell death/apoptosis genes in *Tigit⁻/⁻* cells, such as *Ciapin1* and *Dapk2* (Figure 2f, g). These findings reveal that TIGIT significantly influences transcriptional changes in CD4⁺ T cells during infection, warranting deeper exploration. This suggests a nuanced role for TIGIT, potentially in modulating T-cell activation and survival, offering new insights into its function and its impact on host defense mechanisms.

Anti-TIGIT therapy provides antibacterial benefit

Monoclonal antibodies targeting TIGIT have shown potential in preclinical models of cancer therapy and are currently undergoing clinical trials for multiple cancer types.[21] To investigate whether anti-TIGIT blockade could also prove effective in enhancing antibacterial immunity, mice under *S.* Typhimurium infection were treated every 3 days with a blocking anti-TIGIT antibody (clone 10A7, mIgG2a)[10] or isotype control (Figure 3a). Of note, we observed a significant reduction in bacterial load in the spleens of anti-TIGIT–treated compared with isotype control–treated animals (Figure 3b), indicating that anti-TIGIT treatment can enhance antibacterial immunity. No differences were observed in bacterial burdens in the liver (Supplementary figure 3a). When examining the immune populations by flow cytometry, we found that while TIGIT could be detected as expected on a large proportion of CD4⁺ T cells from the isotype control–treated mice, TIGIT could not be detected on cells of mice treated with anti-TIGIT therapy (Supplementary figure 3b). We speculated that this could be due to either depletion of TIGIT⁺ cells by antibody-dependent cellular cytotoxicity/phagocytosis or blocking of TIGIT by the therapeutic antibody, thereby preventing binding by the flow antibody (clone 1G9). When looking at the total cell numbers in spleens of anti-TIGIT–treated mice compared with isotype control–treated mice, we found no reduction in CD4⁺ T-cell numbers, including CD4⁺ T_{conv} (Figure 3c) or T_{reg} (Figure 3d, e), suggesting that our antibody was not depleting TIGIT⁺ cells. We also saw no differences in the total numbers of other effector lymphocytes including natural killer cells or CD8⁺ T cells in the spleen of treated animals (Supplementary figure 3c, d). When splenocytes isolated from infected mice were pretreated with the therapeutic antibody before flow staining, we could not detect the expression of TIGIT, confirming that the therapeutic antibody can prevent *ex vivo* staining by the flow antibody. Regardless, anti-TIGIT therapy lowered bacterial burdens in the spleen of infected mice.

To assess whether TIGIT was limiting IFNγ production *in vivo* as we observed *in vitro*, CD4⁺ T cells were isolated from treated mice, stimulated for 4 h with PMA/ionomycin and then stained for IFNγ and tumor necrosis factor expression (Figure 3f). We found no differences in the expression of either cytokine from anti-TIGIT-treated mice compared with isotype control (Figure 3g, Supplementary figure 3e). Further, when examining the IFNγ titers from the serum of treated mice, we found no differences in IFNγ levels at either day 5 (Figure 3h) or day 12 (Figure 3i) postinfection. Taken together, these data suggest that anti-TIGIT therapy can enhance antibacterial immune responses independently of depletion of suppressive T_{reg} cells or increases in IFNγ production.

Figure 2. Deletion of TIGIT induces transcriptional changes in CD4$^+$ T cells. WT or *Tigit*$^{-/-}$ CD4$^+$ T cells from naïve or day 10 *S*. Typhimurium–infected BM chimeras were sorted and processed for RNA extraction, library preparation and sequencing. **(a)** Normalized counts of *Tigit* across experimental groups. **(b)** Venn diagram of differentially expressed genes shared between naïve WT and *Tigit*$^{-/-}$ and infected WT and *Tigit*$^{-/-}$. **(c)** Heatmap showing relative expression (*z*-scores) of all differentially expressed genes between infected WT and *Tigit*$^{-/-}$ CD4$^+$ T cells ($P_{adj} < 0.05$ and log$_2$FC > 0.58). **(d, e)** GSEA barcode plots of **(d)** hallmark MTORC1 or **(e)** G2M checkpoint signaling pathways in *Tigit*$^{-/-}$ *versus* WT CD4$^+$ T cells. **(f, g)** Normalized counts of selected differentially expressed genes. Each symbol represents an individual mouse. Data are from two independent experiments ($n = 12$). Graphs show median ± interquartile range. Groups were compared by the Wald test with Benjamini–Hochberg adjustment for **(b)** and **(c)**, or the Mann–Whitney *U*-test with Benjamini, Krieger and Yekutieli adjustment for multiple comparisons for **(a)**, **(f)** and **(g)**, where *P* < 0.05 was considered significantly different. BM, bone marrow; ES, enrichment score; FC, fold change; FDR, false discovery rate; GSEA, Gene Set Enrichment Analysis; KO, knock out; mTORC1, mammalian target of rapamycin complex 1; T$_{reg}$, regulatory T cells; TIGIT, T-cell immunoglobulin and ITIM domain; WT, wild type.

A functional Fc region promotes the antibacterial effect of anti-TIGIT therapy

Fragment crystallizable (Fc) receptors are stimulatory immune receptors that exert functions upon binding to the Fc region of antibodies. The importance of Fc-binding capacity for anti-TIGIT therapy is unclear,[22,23] with some clinical trials in cancers utilizing enhanced Fc regions, while others opting for disabled Fc regions.[21] Therefore, to investigate the need for Fc functionality in our model, we generated anti-TIGIT clone 10A7 antibodies with well-characterized mutations to silence (N297Q)[24] or enhance (S241D.A332L.I334E)[25] binding to Fc receptors. We used a Biacore assay to confirm the Fc-binding capacity of these antibodies to $Fc\gamma R1$, $Fc\gamma R2$ or $Fc\gamma R4$. Notably, the 10A7-Silent antibody was unable to bind to any of the receptors (Supplementary figure 4a–c), whereas the 10A7-WT (Supplementary figure 4d–f) and 10A7-Enhanced demonstrated binding to all three (Supplementary figure 4g–i). A comparison of the maximum binding of each antibody–receptor combination showed that the 10A7-Enhanced had stronger binding compared with the 10A7-WT for each receptor (Supplementary figure 4j–l). Thus, the Fc portion of each antibody was functioning as intended.

We then used these antibodies to treat *S.* Typhimurium–infected mice with the same schedule as previously performed (Figure 4a). Notably, both 10A7-WT and 10A7-Enhanced treatments were able to significantly reduce splenic bacterial burdens compared with isotype control, whereas 10A7-Silent was not (Figure 4b), suggesting that Fc binding promotes anti-TIGIT functionality. Once again, we found that none of the anti-TIGIT antibodies could reduce bacterial burdens in the liver of infected mice (Supplementary figure 5a), nor deplete T_{conv} (Figure 4c) or T_{reg} (Figure 4d, e) within the spleen compared with isotype. However, both 10A7-WT and 10A7-Enhanced treatment led to reduced numbers of T_{conv} and T_{reg} when compared with 10A7-Silent. To assess functional changes in response to treatment, we also examined levels of various effector cytokines in the serum of treated mice. At day 5 postinfection, we found that mice treated with 10A7-Enhanced had a significant increase in titers of inflammatory cytokines $IFN\gamma$ (Figure 4f) and tumor necrosis factor (Figure 4g), as well as the chemokine macrophage inflammatory protein-1 beta (MIP-1β; Figure 4h), compared with isotype- or 10A7-Silent–treated mice. However, these differences were no longer apparent by day 12 postinfection (Supplementary figure 5b–d). Considering the importance of these cytokines in controlling bacterial infection, we predicted that an increase in these cytokines could play an important role in reducing bacterial burdens. Together, these data show that a functional Fc region promotes the functionality of anti-TIGIT, suggesting a mechanism beyond the enhancement of T-cell function solely through direct blocking of TIGIT–CD155 interactions.

TIGIT blockade worsens *M. tuberculosis* infection

While *Salmonella* infection is a meaningful cause of mortality in humans, tuberculosis (an infection caused by *Mycobacterium tuberculosis*) is the leading cause of death by a bacterial agent worldwide. To examine whether anti-TIGIT therapy may also be relevant as a treatment for tuberculosis, we took advantage of a publicly available data set of lymphocytes isolated from *M. tuberculosis*–infected murine lungs.[26] We isolated the $CD4^+$ T cells from this data set and found we could cluster the cells into the same populations as the original paper: naïve, activated 1, activated 2, IFN responsive and T_{reg} (Supplementary figure 6a). Notably, we found an upregulation in TIGIT expression in the T_{reg} and activated 1 clusters at both day 50 and day 100 postinfection compared with naïve mice (Supplementary figure 6a), suggesting that TIGIT may be an appropriate target for immunotherapy in tuberculosis. To investigate this, mice were infected with *M. tuberculosis* and treated with anti-TIGIT antibodies twice weekly starting at 2 weeks postinfection. At day 45, spleens and lungs were taken for histology and enumeration of bacterial burden. We found no difference in lung pathology between the treatment groups (Supplementary figure 6c, d). Interestingly, bacterial burdens from both the spleen (Supplementary figure 6e) and lung (Supplementary figure 6f) were increased following treatment with either 10A7-Silent or 10A7-WT. Together, this suggests that while anti-TIGIT therapy may be suitable for the treatment of some bacterial infections, this therapy may worsen outcomes in others.

DISCUSSION

TIGIT is an inhibitory immune checkpoint that has shown promise as a target for immunotherapy in cancer. In this study, we show that TIGIT also limits immunity during *S.* Typhimurium infection, and anti-TIGIT monotherapy can enhance immune responses to reduce bacterial burdens. However, the efficacy of anti-TIGIT in many other bacterial infections remains unknown and should not be assumed. This is particularly important when considering that targeting the PD-1/programmed death-ligand 1 (PD-L1) pathway shows promise in the treatment of *Pseudomonas aeruginosa* and *Staphylococcus aureus* infection,[27] whereas targeting this same pathway
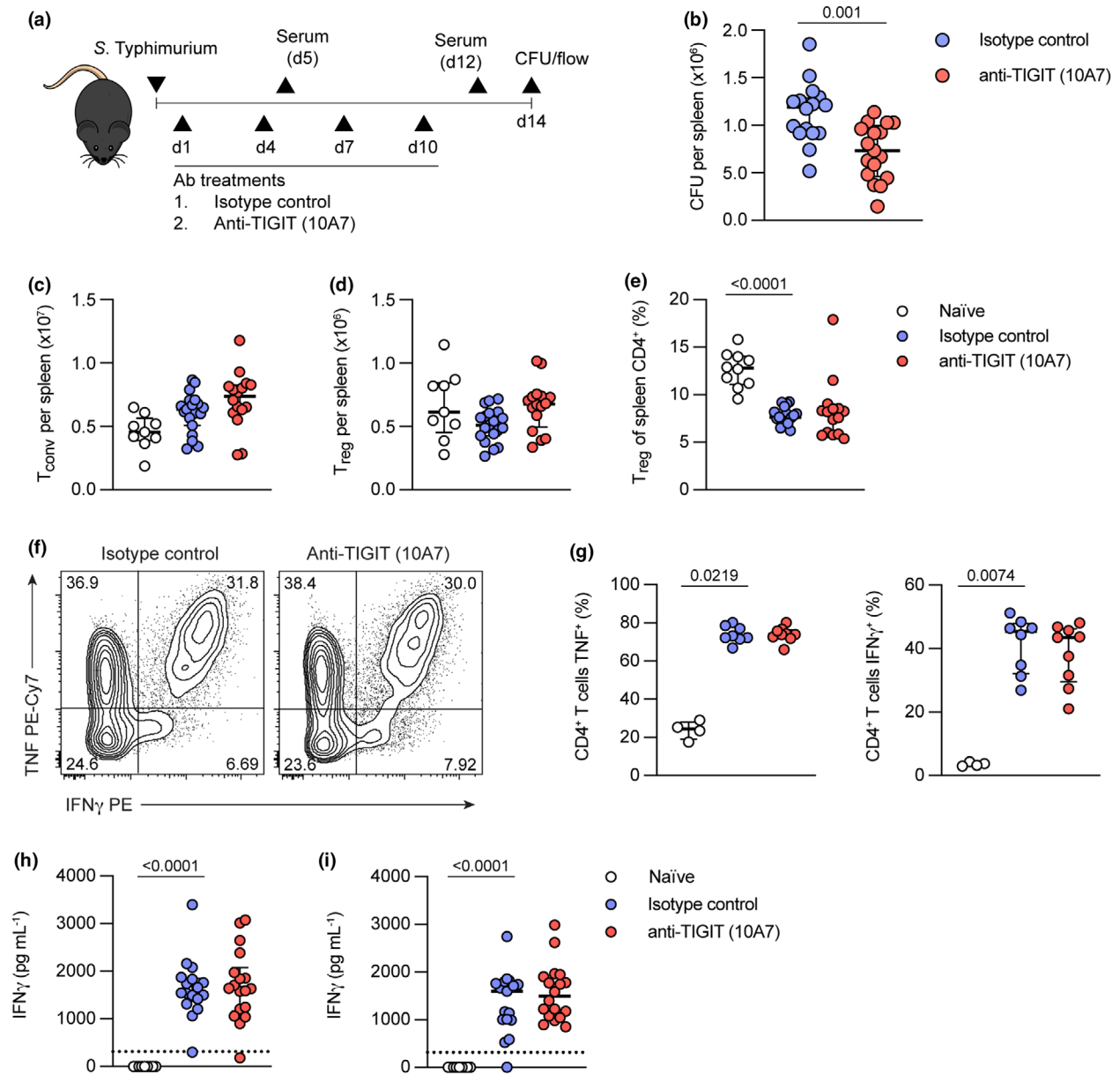
Figure 3. Anti-TIGIT therapy provides antibacterial benefits. Mice under *S.* Typhimurium infection were treated with anti-TIGIT (clone 10A7) or isotype control every 3 days. On day 14, spleens were taken to quantify bacterial burden and immune parameters. **(a)** Schematic showing experimental design. **(b)** Bacterial burdens in the spleen of infected mice. **(c, d)** Total number of T_{conv} **(c)** and T_{reg} **(d)** in the spleens of experimental mice. **(e)** T_{reg} as a percentage of total CD4$^+$ T cells. **(f)** Representative flow plot of cytokine staining in CD4$^+$ T cells from infected mice. **(g)** Percentage of CD4$^+$ T cells expressing either TNF or IFNγ. **(h, i)** IFNγ titers in the serum of experimental animals at day 5 **(h)** or day 12 **(i)** postinfection. Each symbol represents an individual mouse. Data are from two independent experiments for **(b–e)**, **(h)** and **(i)** (n = 9–19), or a single experiment representative of two independent experiments for **(f)** and **(g)** (n = 4–8). Graphs show median ± interquartile range. Groups were compared by the Mann–Whitney U-test, where $P < 0.05$ was considered significantly different. Ab, antibody; IFNγ, interferon gamma; T_{conv}, conventional T cells; T_{reg}, regulatory T cells; TIGIT, T-cell immunoglobulin and ITIM domain; TNF, tumor necrosis factor.

drastically exacerbates *M. tuberculosis* infection.[28–30] Indeed, we show that anti-TIGIT therapy does not reduce spleen or lung burdens during *M. tuberculosis* infection,

and even leads to exacerbation of bacterial burden in the lung. Conversely, targeting Tim-3 in murine models of *M. tuberculosis* has been shown to be effective in reducing
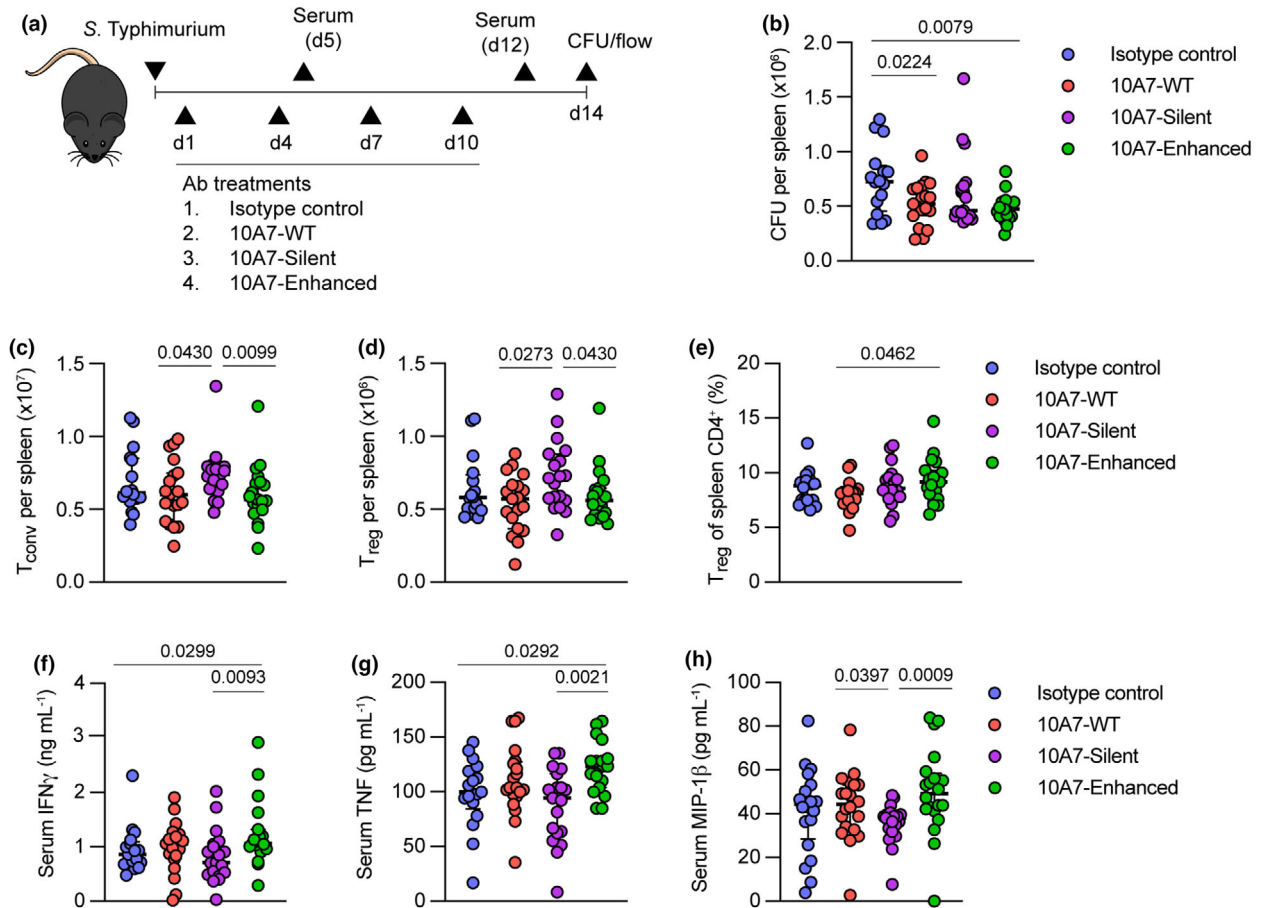
Figure 4. Anti-TIGIT effect on bacterial burden requires a functional Fc region. Mice under *S.* Typhimurium infection were treated with mutant anti-TIGIT antibodies (clone 10A7) or isotype control every 3 days. At day 14, spleens were taken to quantify bacterial burden and immune parameters. **(a)** Schematic showing experimental design. **(b)** Bacterial burdens in the spleen of infected mice. **(c, d)** Total number of T_{conv} **(c)** and T_{reg} **(d)** in the spleens of experimental mice. **(e)** T_{reg} as a percentage of total $CD4^+$ T cells. **(f–h)** Titers of **(f)** IFNγ, **(g)** TNF and **(h)** MIP-1β in the serum of infected mice at day 5 postinfection. Each symbol represents an individual mouse. Data are from two independent experiments ($n = 16$–19). Graphs show median $\pm$ interquartile range. Groups were compared by the Mann–Whitney U-test, where $P < 0.05$ was considered significantly different. Ab, antibody; IFNγ, interferon gamma; MIP-1β, macrophage inflammatory protein-1 beta; T_{conv}, conventional T cells; TIGIT, T-cell immunoglobulin and ITIM domain; TNF, tumor necrosis factor; T_{reg}, regulatory T cells; WT, wild type.

bacterial burdens.[31] These results highlight the complicated interplay between different bacterial pathogens and the host immune response, showing that pathogens may require targeting of different mechanisms to prevent the risk of disease exacerbation.

Immune checkpoints such as TIGIT downregulate immune function when interacting with their ligand, suggesting that immune checkpoint inhibition works through interruption of the checkpoint–ligand interaction. A key finding of this study was that an enhanced Fc region of the anti-TIGIT antibody promotes its functionality, which does not support the interruption of the checkpoint–ligand interaction hypothesis.

Fc-dependent depletion of suppressive T_{reg} has previously been reported to be necessary for the anticancer efficacy of anti–CTLA-4.[32] In our hands, T_{reg} depletion was not evident in the spleen in response to anti-TIGIT therapy, suggesting that T_{reg} depletion was not responsible for reducing bacterial burden (however, functional changes in T_{reg} were not examined and should not be disregarded). Preclinical cancer models have also shown that anti-TIGIT therapy is dependent on a functional Fc region and FcγR4, yet the therapy does not deplete intratumoral T_{reg}.[22,33] Instead, anti-TIGIT therapy may work through either enhancing the proinflammatory function of Fc receptor–expressing cells or enforcing a

stronger synapse between Fc receptor–expressing antigen-presenting cells and T cells. Indeed, a recent clinical study found that anti-TIGIT therapy was associated with clinical benefit in tumors that were highly infiltrated with myeloid cells and T_{reg} and that this therapy was able to activate peripheral myeloid cells such as monocytes.[34] These hypotheses are strengthened by studies showing that TIGIT$^{-/-}$ mice have no antitumor benefit compared with WT mice.[33] When considering anti-TIGIT functionality, blocking the TIGIT–CD155 interaction could work in concert with Fc binding to exert its effect, or TIGIT itself could to some degree be irrelevant and primarily act as an anchor point to allow antibodies to tether effector T cells to FcγR4-expressing myeloid cells. Regardless, determining the mechanism of anti-TIGIT should be of utmost importance to effectively engineer the antibody to maximize benefit and prevent investment in unnecessary clinical trials. To our knowledge, there are currently 13 clinical trials investigating anti-TIGIT antibodies in cancer therapy, some of which are using disabled Fc regions and others using enhanced Fc regions,[21] highlighting the lack of mechanistic understanding behind anti-TIGIT therapy.

The importance of anti-TIGIT Fc functionality may also explain previous inconclusive data on TIGIT in infectious diseases. One study used TIGIT$^{-/-}$ mice to show that TIGIT expression does not dampen natural killer cell or T-cell responses during *Toxoplasma gondii* infection[35]; however, that study did not utilize anti-TIGIT antibodies. Another study showed that during lymphocytic choriomeningitis virus infection, engagement of TIGIT limited proinflammatory tumor necrosis factor and IFNγ production and upregulated anti-inflammatory IL-10 production, while it did not alter viral titers.[15] Importantly, the lymphocytic choriomeningitis virus study used an mIgG1 antibody, which does not bind to FcγR4,[36] the Fc receptor found to be critical for anti-TIGIT function in cancer models. Both studies are consistent with the cancer data showing genetic deletion of TIGIT provides no benefit, and engagement of FcγR4 is required for anti-TIGIT therapy. It is, therefore, plausible to speculate that therapeutic benefit could be observed in both models if they had taken advantage of an FcγR4-competent antibody, and it remains to be seen if anti-TIGIT therapy is viable in parasitic and viral diseases. TIGIT has also been implicated in the pronounced immunosuppression during sepsis[37–39]; however, to our knowledge, TIGIT blockade has not yet been trialed in either humans or mouse models of sepsis. Considering the substantial global health burden posed by sepsis, which has been estimated to be associated with 19.7% of all global deaths,[40] immunotherapies such as anti-TIGIT should be investigated.

In conclusion, here we have shown that TIGIT marks effector lymphocytes during *S.* Typhimurium infection, and anti-TIGIT therapy is able to enhance bacterial control. We further show that enhancing Fc binding promotes the therapeutic effect of anti-TIGIT therapy. However, our results in tuberculosis highlight that the effectiveness of anti-TIGIT should not be generalized for all bacterial infections and warrant further study in different infection models. Thus, inhibition of immune checkpoints such as TIGIT may provide a novel avenue for the treatment of some bacterial infections, which could be important in cases of antibiotic resistance where treatment options are limited.

METHODS

Mice

C57BL/6J and B6.SJL-Ptprca (CD45.1) mice were purchased from the Animal Resources Centre or Australian Bioresources and housed at the Biological Resources Facility of the Translational Research Institute or the Australian Institute of Tropical Health and Medicine at James Cook University. *Tigit*$^{-/-}$ mice were bred and maintained at the QIMR Berghofer Medical Research Institute. Mice for *in vivo* studies were female aged 8–12 weeks, while mice for *in vitro* studies were from either gender aged 8–12 weeks. All mice were bred and housed in specific pathogen-free conditions in ventilated cages under a 12-h light cycle. All animal experiments were conducted according to approval by the University of Queensland Health Science Animal Ethics Committee (approval numbers 2019/AE000536 and 2021/AE000585) and the Animal Ethics Committee of James Cook University (A2837). All procedures were carried out in accordance with the regulatory standards of the National Health and Medical Research Council (NHMRC) and the Australian Code for the Responsible Conduct of Research.

Bacterial strains and *in vivo* infections

Mice were infected with an attenuated *aroA* mutant strain of *Salmonella enterica* subspecies Typhimurium, SL3261.[41] For *in vivo* infection, bacteria were grown at 37°C with shaking in Lysogeny broth for 16–18 h. OD$_{600}$ (optical density at 600 nm) was used to enumerate bacteria, before being diluted to the appropriate concentration in phosphate-buffered saline (PBS). Mice received SL3261 at 1×10^6 CFU in 200 μL by intraperitoneal injection.

For *M. tuberculosis* infection, mice were infected with 20–50 CFU of *M. tuberculosis* H37Rv using a Glas-Col inhalation exposure system in the Biosafety Level 3 laboratory at James Cook University. Before loading the Glas-Col nebulizer system, frozen *M. tuberculosis* stocks were thawed, diluted to the appropriate concentration and treated in an ultrasound water bath to disrupt bacterial clumps. One day after the aerosol infection, five mice were killed, and the

lung tissue was plated on 10% oleic albumin dextrose catalase–enriched 7H11 agar plates (BD Biosciences, Franklin Lakes, NJ, USA) to determine the infectious dose.

In vivo treatments

The sequence of anti-TIGIT clone 10A7 was taken from the US patent number 9499596 and cloned onto a mIgG2a backbone. Fc-silent and Fc-enhanced variants were generated by introducing N297A and S241D.A332L.I334E mutations into the Fc region. Anti-TIGIT antibodies for *in vivo* use were generated by the National Biological Facility (University of Queensland, Australia). *S.* Typhimurium–infected mice were treated via intraperitoneal administration of 200 μg of anti-TIGIT antibodies or isotype control (anti-gp120, mIgG2a) every 3 days starting at day 1 postinfection. *Mycobacterium tuberculosis*–infected mice were treated via intraperitoneal administration of 200 μg of anti-TIGIT antibodies or isotype control (anti-gp120, mIgG2a, National Biological Facility, University of Queensland, Australia) twice weekly starting at 2 weeks postinfection.

Biacore binding assay

The binding of the antibodies to mouse Fc gamma receptors was evaluated using surface plasmon resonance (SPR) on a Biacore 8K+ instrument. The His-tagged receptors were purchased from Sino Biological (Beijing, China): FCGR1 (50086-M08H), FCGR3 (50326-M08H) and FCGR4 (50036-M08H). The receptors at 0.3 μg mL^{-1} were captured (~100–200 RU) onto Flow Cell 2 of a CM5 chip previously coated with anti-His antibody [coated as per His Capture Kit instructions (Cytiva, Marlborough, MA, USA)]. Each antibody was then injected over both flow cells for 180 s at 30 μL min^{-1} followed by a 600-s dissociation phase. The antibodies were injected at serial 1:2 dilutions (starting at 111 nM) with a regeneration using 10 mM glycine (pH 1.5) between each concentration. A zero-concentration cycle was included to allow double-reference subtraction (Fc2–Fc1 and zero analyte subtraction). Biacore Insight Evaluation was used to fit 1:1 binding kinetics and affinity models.

Murine tissue collection

Blood samples were taken from mice by retro-orbital bleeds into ethylenediaminetetraacetic acid (EDTA)–coated tubes. Tubes were centrifuged at 1500 *g* for 15 min, and serum was removed from the cell pellet. Serum samples were stored at −20°C until analysis. At the experimental endpoint, mice were killed by CO_2 asphyxiation. Organs were dissected and held in PBS until processing. Bacterial counts were enumerated from organs by homogenizing samples in 0.1% Triton-X (Sigma-Aldrich, St. Louis, MO, USA) in PBS before serially diluting in PBS and plating on lysogeny broth agar plates.

From *M. tuberculosis*–infected mice, the right lung lobes were used for CFU enumeration and the left lung lobe was used for histopathology. Lung and spleen tissues were homogenized in gentleMACS tubes (Miltenyi Biotec, Bergisch Gladbach, Germany) containing 1 mL of sterile PBS/0.05% Tween 80 (Sigma-Adrich). Tenfold dilutions of organ homogenates were plated onto Middlebrook 7H11 agar plates supplemented with 0.2% glycerol (Sigma-Aldrich), 0.05% Tween-80 (Sigma-Aldrich) and 10% oleic albumin dextrose catalase enrichment (BD Biosciences). Agar plates were sealed and incubated aerobically at 37°C. Colonies were counted at 3 and 5 weeks and the total CFU per organ was calculated based on dilution factor and organ size.

Histopathology

Left lung lobes from *M. tuberculosis*–infected C57BL/6 mice were fixed overnight with 10% w/v neutral buffered formalin (Proscitech, Queensland, Australia), transferred to 70% ethanol and embedded in paraffin. Processed lungs were sectioned into 4-μm slices, transferred to microscope slides, dewaxed and stained with hematoxylin (Sigma-Aldrich) and eosin (Proscitech). Stained slides were scanned with an Aperio LV1 (Leica, Wetzlar, Germany) followed by analysis with ImageJ software (version 1.54g, NIH, Bethesda, MD, USA) and QuPath (versions 0.2.3 and 0.4.4).[42] To calculate the percentage of lung damage, the total surface area was compared with the areas of dense cell infiltration.

Flow cytometry

Spleens were passed through a 70-μm cell strainer in cold fluorescence-activated cell sorting (FACS) buffer (PBS containing 2% fetal bovine serum and 2 mM EDTA). Leukocytes were enriched using 37.5% Percoll solution (GE HealthCare, Chicago, IL, USA) and red blood cells lysed with ammonium-chloride–potassium lysis buffer (Biolegend, San Diego, CA, USA). Fc receptors were blocked by incubation for 15 min in Fc blocking reagent (1:100 in FACS buffer; Miltenyi Biotec). Single-cell suspensions were stained with the indicated fluorescent antibodies on ice for 45 min. For intracellular cytokine staining, cells were fixed and permeabilized using the FoxP3/Transcription Factor Staining Buffer Set (eBioscience, San Diego, CA, USA) and then stained for 60 min with the indicated fluorescent antibodies. Antibodies targeting CD45 (30-F11), CD4 (GK1.5), CD3 (145-2C11), CD8a (53-6.7), TIGIT (1G9), CD69 (H1.2F3), CD223 (C9B7W), CD49b (HMa2), CD44 (IM7), PD-1 (J43) and NK1.1 (PK136) were purchased from Becton Dickinson (Franklin Lakes, NJ, USA). Antibodies targeting CD103 (2E7), CD226 (TX42.1), CD335 (29A1.4), KLRG1 (2F1/KLRG1), CD19 (6D5), Ly6G (1A8), F4/80 (BM8), Ki-67 (16A8) and CD62L (MEL-14) were purchased from BioLegend. Antibodies targeting Tim-3 (RMT3-23), Eomes (Dan11mag) and FoxP3 (FJK-16S) were purchased from eBioscience. Data were acquired on a BD FACSymphony A5 (BD Biosciences) or a Cytek Aurora (Cytek Biosciences, Fremont, CA, USA). Flow cytometry data analysis was performed using FlowJo software (version 10.9, Tree Star, San Carlos, CA, USA).

Measurement of cytokines

IFNγ titers were determined from murine serum samples using a mouse IFNγ ELISA set (BD Biosciences) as per the manufacturer's instructions. Other cytokines were determined using Cytometric Bead Array (BD Biosciences) as per the manufacturer's instructions.

T-cell *ex vivo* stimulation

To obtain single-cell suspensions, spleens were passed through a 70-µM cell strainer in FACS buffer (PBS containing 2% fetal calf serum and 2 mM EDTA). To enrich CD4 T cells, splenocytes were stained with biotinylated antibodies targeting Ly6G, F4/80, Ter119, CD19, CD8 and MHC-II (BioLegend); mixed with magnetic streptavidin beads; and separated on an EasySep magnet (StemCell Technologies, Vancouver, BC, Canada). Supernatants were stained with fluorescent antibodies targeting CD3, CD4 and CD25, and viable $CD3^+CD4^+CD25^-$ cells were isolated on an FACS ARIA Fusion flow cytometer (BD Biosciences). $CD4^+$ T cells were plated at 200 000 cells per well in the presence of plate-bound anti-CD3 (5 µg mL^{-1}, Invitrogen, Waltham, MA, USA) and anti-CD28 (2 µg mL^{-1}, Invitrogen) in 96-well plates containing Roswell Park Memorial Institute-1640 (RPMI-1640; Gibco, Carlsbad, CA, USA) supplemented with 10% fetal calf serum, 1% non-essential amino acids (Gibco), 1% sodium pyruvate (Gibco), 1% GlutaMAX (Gibco), 1% penicillin–streptomycin (Gibco) and 0.1% 2-mercaptoethanol (Gibco). In some cases, T cells were also incubated in the presence of plate-bound CD155-Fc (R&D Systems, Minneapolis, MN, USA) or human immunoglobulin G isotype control. Plates were incubated at 37°C with 5% CO_2 for 24–72 h as indicated in the figure captions.

Generation of bone marrow chimeras

Four-week-old recipient CD45.1 mice were sublethally irradiated with two doses of 550 cGy 3 h apart. Four hours after the second dose of irradiation, mice were injected intravenously with a 50:50 mix of bone marrow cells from WT CD45.1.2 and *Tigit*$^{-/-}$ (CD45.2) mice. Mice were maintained on neomycin water for at least 3 weeks and used for experimentation 8–10 weeks after reconstitution.

Bulk RNA-sequencing

Samples were sorted by flow cytometry and RNA was isolated using the Maxwell RSC simplyRNA Cells RNA Extraction Kit (Promega, Madison, WI, USA) as per the manufacturer's instructions. Libraries were prepped using an Illumina Stranded mRNA prep Kit (Illumina, San Diego, CA, USA) and sequenced on a NovaSeq6000 platform (single end, 100 bp). The reads were mapped to the mouse genome (mm10) using HISAT2. Transcripts were then assembled and quantified using StringTie. Differential expression analysis was performed using DESeq2. Genes with a log$_2$ fold change of 0.58 and adjusted *P*-value of < 0.05 were considered significantly differentially expressed.

Data analysis

Statistical analyses were performed in GraphPad Prism (version 10, GraphPad Software, La Jolla, CA, USA). Data are presented as median + interquartile range. The Mann–Whitney *U*-test was used to compare unpaired groups, whereas the Wilcoxon matched-pairs singed-rank test was used to compare paired groups, as indicated in figure captions. $P < 0.05$ was considered significantly different, and significant *P*-values are marked in the figures. Where possible, experiments were performed blinded until after data analysis was performed.

The Spectre package for R (R Foundation, Vienna, Austria) was used to perform t-distributed stochastic neighbor embedding analysis of flow cytometry data.[43] Samples were initially prepared in FlowJo, and the populations of interest were exported as batch value CSV files. The data set was then merged into a single data table, with keywords denoting the sample, group and other factors added to each row (cell). The FlowSOM algorithm[44] was then run on the merged data set to cluster the data, where every cell is assigned to a specific cluster and metacluster. Subsequently, the data were downsampled and analyzed by the dimensionality reduction algorithm (t-distributed stochastic neighbor embedding).[45]

AUTHOR CONTRIBUTIONS

Timothy R McCulloch: Conceptualization; data curation; formal analysis; investigation; methodology; project administration; writing – original draft; writing – review and editing. **Gustavo R Rossi:** Conceptualization; investigation; resources. **Socorro Miranda-Hernandez:** Formal analysis; investigation; methodology; resources. **Ana Maria Valencia-Hernandez:** Methodology; resources; visualization. **Louisa Alim:** Investigation; methodology. **Clemence J Belle:** Data curation; investigation. **Andrew Krause:** Methodology; resources. **Lucia F Zacchi:** Methodology; resources. **Pui Yeng Lam:** Investigation; methodology. **Kyohei Nakamura:** Resources. **Andreas Kupz:** Methology; resources; investigation; supervision. **Timothy J Wells:** Investigation; supervision. **Fernando Souza-Fonseca-Guimaraes:** Conceptualization; funding acquisition; investigation; methodology; project administration; resources; supervision; writing – original draft.

CONFLICT OF INTEREST

The authors declare they have no competing interests.

DATA AVAILABILITY STATEMENT

RNA-sequencing data are available as raw or processed files in the NCBI GEO database under accession number GSE234086.

REFERENCES

1. Murray CJL, Ikuta KS, Sharara F, et al. Global burden of bacterial antimicrobial resistance in 2019: a systematic analysis. *Lancet* 2022; **399**: 629–655.

2. McCulloch TR, Wells TJ, Souza-Fonseca-Guimaraes F. Towards efficient immunotherapy for bacterial infection. *Trends Microbiol* 2022; **30**: 158–169.

3. Wykes MN, Lewin SR. Immune checkpoint blockade in infectious diseases. *Nat Rev Immunol* 2018; **18**: 91–104.

4. Dyck L, Mills KHG. Immune checkpoints and their inhibition in cancer and infectious diseases. *Eur J Immunol* 2017; **47**: 765–779.

5. He X, Xu C. Immune checkpoint signaling and cancer immunotherapy. *Cell Res* 2020; **30**: 660–669.

6. Chamoto K, Hatae R, Honjo T. Current issues and perspectives in PD-1 blockade cancer immunotherapy. *Int J Clin Oncol* 2020; **25**: 790–800.

7. Rowshanravan B, Halliday N, Sansom DM. CTLA-4: a moving target in immunotherapy. *Blood* 2018; **131**: 58–67.

8. Anderson AC, Joller N, Kuchroo VK. Lag-3, Tim-3, and TIGIT: co-inhibitory receptors with specialized functions in immune regulation. *Immunity* 2016; **44**: 989–1004.

9. Harjunpää H, Guillerey C. TIGIT as an emerging immune checkpoint. *Clin Exp Immunol* 2020; **200**: 108–119.

10. Yu X, Harden K, Gonzalez LC, et al. The surface protein TIGIT suppresses T cell activation by promoting the generation of mature immunoregulatory dendritic cells. *Nat Immunol* 2009; **10**: 48–57.

11. Johnston RJ, Comps-Agrar L, Hackney J, et al. The immunoreceptor TIGIT regulates antitumor and antiviral CD8$^+$ T cell effector function. *Cancer Cell* 2014; **26**: 923–937.

12. Stanietsky N, Simic H, Arapovic J, et al. The interaction of TIGIT with PVR and PVRL2 inhibits human NK cell cytotoxicity. *Proc Natl Acad Sci USA* 2009; **106**: 17858–17863.

13. Joller N, Lozano E, Burkett PR, et al. Treg cells expressing the coinhibitory molecule TIGIT selectively inhibit proinflammatory Th1 and Th17 cell responses. *Immunity* 2014; **40**: 569–581.

14. Ge Z, Peppelenbosch MP, Sprengers D, Kwekkeboom J. TIGIT, the next step towards successful combination immune checkpoint therapy in cancer. *Front Immunol* 2021; **12**: 699895.

15. Schorer M, Rakebrandt N, Lambert K, et al. TIGIT limits immune pathology during viral infections. *Nat Commun* 2020; **11**: 1288.

16. Chew GM, Fujita T, Webb GM, et al. TIGIT marks exhausted T cells, correlates with disease progression, and serves as a target for immune restoration in HIV and SIV infection. *PLoS Pathog* 2016; **12**: 1–28.

17. Mellinghoff SC, Thelen M, Bruns C, et al. T-cells of invasive candidiasis patients show patterns of T-cell-exhaustion suggesting checkpoint blockade as treatment option. *J Infect* 2022; **84**: 237–247.

18. Cook L, Munier CML. Help is on the way: critical roles of CD4$^+$ T cells in infection and vaccination. *Immunol Cell Biol* 2023; **101**: 489–490.

19. Salazar GA, Peñaloza HF, Pardo-Roa C, et al. Interleukin-10 production by T and B cells is a key factor to promote systemic *salmonella enterica* serovar typhimurium infection in mice. *Front Immunol* 2017; **8**: e889.

20. Joller N, Hafler JP, Brynedal B, et al. Cutting edge: TIGIT has T cell-intrinsic inhibitory functions. *J Immunol* 2011; **186**: 1338–1342.

21. Dolgin E. Antibody engineers seek optimal drug targeting TIGIT checkpoint. *Nat Biotechnol* 2020; **38**: 1007–1009.

22. Waight JD, Chand D, Dietrich S, et al. Selective FcγR co-engagement on APCs modulates the activity of therapeutic antibodies targeting T cell antigens. *Cancer Cell* 2018; **33**: 1033–1047.

23. Chen X, Xue L, Ding X, et al. An Fc-competent anti-human TIGIT blocking antibody ociperlimab (BGB-A1217) elicits strong immune responses and potent anti-tumor efficacy in pre-clinical models. *Front Immunol* 2022; **13**: e828319.

24. Walker MR, Lund J, Thompson KM, Jefferis R. Aglycosylation of human IgG1 and IgG3 monoclonal antibodies can eliminate recognition by human cells expressing FcγRI and/or FcγRII receptors. *Biochem J* 1989; **259**: 347–353.

25. Lazar GA, Dang W, Karki S, et al. Engineered antibody Fc variants with enhanced effector function. *Proc Natl Acad Sci USA* 2006; **103**: 4005–4010.

26. Akter S, Chauhan KS, Dunlap MD, et al. *Mycobacterium tuberculosis* infection drives a type I IFN signature in lung lymphocytes. *Cell Rep* 2022; **39**: 110983.

27. Patil NK, Luan L, Bohannon JK, Hernandez A, Guo Y, Sherwood ER. Frontline science: anti-PD-L1 protects against infection with common bacterial pathogens after burn injury. *J Leukoc Biol* 2018; **103**: 23–33.

28. Barber DL, Mayer-Barber KD, Feng CG, Sharpe AH, Sher A. CD4 T cells promote rather than control tuberculosis in the absence of PD-1–mediated inhibition. *J Immunol* 2011; **186**: 1598–1607.

29. Barber DL, Sakai S, Kudchadkar RR, *et al.* Tuberculosis following PD-1 blockade for cancer immunotherapy. *Sci Transl Med* 2019; **11**: eaat2702.

30. Kauffman KD, Sakai S, Lora NE, *et al.* PD-1 blockade exacerbates *Mycobacterium tuberculosis* infection in rhesus macaques. *Sci Immunol* 2021; **6**: eabf3861.

31. Jayaraman P, Jacques MK, Zhu C, *et al.* TIM3 mediates T cell exhaustion during *Mycobacterium tuberculosis* infection. *PLoS Pathog* 2016; **12**: e1005490.

32. Simpson TR, Li F, Montalvo-Ortiz W, *et al.* Fc-dependent depletion of tumor-infiltrating regulatory T cells co-defines the efficacy of anti–CTLA-4 therapy against melanoma. *J Exp Med* 2013; **210**: 1695–1710.

33. Han JH, Cai M, Grein J, *et al.* Effective anti-tumor response by TIGIT blockade associated with FcγR engagement and myeloid cell activation. *Front Immunol* 2020; **11**: 573405.

34. Guan X, Hu R, Choi Y, *et al.* Anti-TIGIT antibody improves PD-L1 blockade through myeloid and Treg cells. *Nature* 2024; **627**: 646–655.

35. Aldridge DL, Phan AT, de Waal Malefyt R, Hunter CA. Limited impact of the inhibitory receptor TIGIT on NK and T cell responses during *Toxoplasma gondii* infection. *Immunohorizons* 2021; **5**: 384–394.

36. Bruhns P. Properties of mouse and human IgG receptors and their contribution to disease models. *Blood* 2012; **119**: 5640–5649.

37. de Lima MHF, Hiroki CH, de Fátima Borges V, *et al.* Sepsis-induced immunosuppression is marked by an expansion of a highly suppressive repertoire of FOXP3+ T-regulatory cells expressing TIGIT. *J Infect Dis* 2022; **225**: 531–541.

38. Sun Y, Ding R, Chang Y, Li J, Ma X. Immune checkpoint molecule TIGIT manipulates T cell dysfunction in septic patients. *Int Immunopharmacol* 2021; **101**: 108205.

39. Washburn ML, Wang Z, Walton AH, *et al.* T cell– and monocyte-specific RNA-sequencing analysis in septic and nonseptic critically ill patients and in patients with cancer. *J Immunol* 2019; **203**: 1897–1908.

40. Rudd KE, Johnson SC, Agesa KM, *et al.* Global, regional, and national sepsis incidence and mortality, 1990–2017: analysis for the global burden of disease study. *Lancet* 2020; **395**: 200–211.

41. Hoiseth SK, Stocker BAD. Aromatic-dependent *Salmonella typhimurium* are non-virulent and effective as live vaccines. *Nature* 1981; **291**: 238–239.

42. Bankhead P, Loughrey MB, Fernández JA, *et al.* QuPath: open source software for digital pathology image analysis. *Sci Rep* 2017; **7**: 16878.

43. Ashhurst TM, Marsh-Wakefield F, Putri GH, *et al.* Integration, exploration, and analysis of high-dimensional single-cell cytometry data using spectre. *Cytometry A* 2022; **101**: 237–253.

44. Van Gassen S, Callebaut B, Van Helden MJ, *et al.* FlowSOM: using self-organizing maps for visualization and interpretation of cytometry data. *Cytometry A* 2015; **87**: 636–645.

45. Van Der Maaten L, Hinton G. Visualizing data using t-SNE. *J Machine Learning R* 2008; **9**: 2579–2605.

SUPPORTING INFORMATION

Additional supporting information may be found online in the Supporting Information section at the end of the article.